Special Feature: Dynamics Modeling Supporting Vehicle Performance

Research Report

Novel Scheme for Implementation of Nonlinear Constitutive Equations into General-purpose Finite Element Software

Masato Tanaka, Takashi Sasagawa and Ryuji Omote

Report received on Aug. 3, 2016

ABSTRACT This report provides an overview of a proposed scheme for the implementation of a broad range of different constitutive equations in general-purpose finite element software, which would help develop multiscale material models. The proposed scheme involves the automatic calculation of stresses and their corresponding tangent moduli using the incremental variational formulation (IVF) and the hyper-dual step derivative (HDSD). The IVF recasts inelasticity theory as an equivalent optimization problem where an incremental effective potential is minimized with respect to various internal variables, e.g., damage, plastic deformations, viscosity, or phase transformations. The current stresses and corresponding tangent moduli can be obtained by differentiating the incremental effective potential with respect to the current deformation gradient. In this study, the HDSD scheme was applied to automatically compute the differentiations needed in the IVF. The proposed implementation scheme has a general structure that is defined such that once the present framework is constructed, any other complicated constitutive equations can be considered by simply modifying scalar-valued quantities, such as the Helmholtz free energy, the dissipation potential, and the yield function in the case of plasticity. By applying it to some material models, the performance of the proposed scheme was demonstrated.

KEYWORDS Finite Element Method, Constitutive Equation, Finite Strain Inelasticity, Incremental Variational Formulation, Hyper-dual Number

1. Introduction

To ensure the safety and reliability of automobiles, the materials used in vehicles must be investigated on both macro- and microscopic levels. In this context, multiscale material modeling has become an active area of computer-aided engineering and has been increasingly applied to the estimation of macroscopic properties from detailed microstructures.[1,2] In multiscale material modeling, especially when the implicit finite element method is used, the exact calculations of stresses and consistent algorithmic tangent moduli are essential to obtain accurate physical results and quadratic convergence, respectively. Most general-purpose finite element software provides a user-defined material subroutine to implement the advanced material models because they include only a finite number of representative and classical material models. However, some novel sophisticated material models result in complex formulations that can be extremely elaborate and error-prone. In such cases, the application of numerical differentiation techniques that can provide robust and accurate results would be an appealing alternative to decrease scientific development time.

Recently, a number of numerical differentiation techniques that can be used to implement various types of material models have been proposed.[3-9] They are based on the implementation scheme by Miehe,[10] which uses the finite difference (FD) method to approximate tangent matrices in finite element formulations. These recently developed techniques enhance the FD approximation by applying more robust and accurate numerical differentiation techniques, such as the complex-step derivative approximation (CSDA). However, such techniques require analytic expressions of the stress tensors, which are still complicated to derive, especially for some advanced hyperelastic or finite strain inelastic material models.

Therefore, this study focused on developing a unifying framework to implement general dissipative material behavior in general-purpose finite element software; the developed framework is the incremental variational formulation (IVF), which was originally proposed by Ortiz and Stainier.[11] The IVF requires the implementation of only scalar functions, such as the

free energy, dissipation potential, and yield law in the case of elastoplasticity, and it is applicable to a broad range of inelastic material models. Furthermore, when scalar functions are implemented within the framework of the IVF, their thermodynamic consistency is a priori guaranteed.[12,13] The main disadvantage of the proposed formulation is that it requires the tedious calculation of the higher-order tensor derivatives. Because the abovementioned CSDA method is applicable to only first-order derivatives, the hyper-dual step derivative (HDSD), a higher-order numerical differentiation scheme proposed by Fike[14] that uses hyper-dual numbers (HDNs), was used in this study. By combining the HDSD with the IVF framework, a fully automatic scheme for the implementation of a broad range of different constitutive equations in general-purpose finite element software was developed. This report reviews previous reports of the proposed formulation[15,16] and demonstrates its performance by applying it to some material models.

2. Numerical Differentiation Techniques

In this section, the numerical differentiation schemes used in this report are summarized based on their application to a simple scalar function $f(x)$. The following Taylor series expansion was considered:

$$f(x+h) = f(x) + hf'(x) + \frac{h^2}{2!}f''(x) + O(h^3), \quad (1)$$

where h denotes a small perturbation and O is Landau's symbol. The classical FD model is obtained by neglecting the higher-order terms $O(h^2)$ as

$$f'_{\mathrm{FD}}(x) \approx \frac{f(x+h) - f(x)}{h}. \quad (2)$$

It is well-known that the FD model is very sensitive to the perturbation value h; a smaller h in Eq. (1) results in a higher accuracy from a strictly mathematical viewpoint but also leads to roundoff errors from a computational viewpoint. To eliminate this undesired sensitivity, Lyness[17] developed the CSDA method. In the CSDA method, the perturbation is multiplied by the imaginary unit i. Replacing h with ih in Eq. (1) and taking only the imaginary part of $f(x+ih)$ yields a different differentiation scheme:

$$f'_{\mathrm{CSDA}}(x) \approx \frac{\Im[f(x+ih)]}{h}, \quad (3)$$

where $\Im$ is an operation symbol that represents taking the imaginary part of the complex argument. This formulation has no roundoff errors even for perturbation values as small as $h = 10^{-99}$.[18] However, it should be noted that the CSDA method is applicable to only first derivatives, not second or higher-order derivatives.

The alternative technique of automatic differentiation (AD), also called algorithmic differentiation, is a set of techniques that can be used to accurately numerically compute derivatives of an arbitrary order with computer precision by repeatedly applying the chain rule.[19] Fike[14] proposed the HDN approach, which is equivalent with forward AD but more intuitive and practical, especially for tensor derivatives. The HDNs of second derivatives have two nilpotent elements ε_1 and ε_2 with the properties:

$$\varepsilon_1^2 = 0, \quad \varepsilon_2^2 = 0, \quad \varepsilon_1\varepsilon_2 = \varepsilon_2\varepsilon_1. \quad (4)$$

Two HDNs $a = (a_1 + a_2\varepsilon_1 + a_3\varepsilon_2 + a_4\varepsilon_1\varepsilon_2)$ and $b = (b_1 + b_2\varepsilon_1 + b_3\varepsilon_2 + b_4\varepsilon_1\varepsilon_2)$ were considered, and $a = b$ was defined if and only if all of their components are equal, i.e., if $a_1 = b_1$, $a_2 = b_2$, $a_3 = b_3$ and $a_4 = b_4$. The operations $\Im_{\varepsilon_1}$, $\Im_{\varepsilon_2}$ and $\Im_{\varepsilon_1\varepsilon_2}$ denote taking the coefficients of the nilpotent elements of the HDNs such that $\Im_{\varepsilon_1}[a] := a_2$, $\Im_{\varepsilon_2}[a] := a_3$ and $\Im_{\varepsilon_1\varepsilon_2}[a] := a_4$. Using the HDNs, Fike[14] developed the HDSD method for a scalar function $f(x)$ by substituting $h\varepsilon_1 + h\varepsilon_2$ for h in Eq. (1). The first derivative $f'(x)$ can be obtained by taking the coefficient of either ε_1 or ε_2 as

$$f'_{\mathrm{HDSD}}(x) = \frac{\Im_{\varepsilon_1}[f(x+h\varepsilon_1+h\varepsilon_2)]}{h} = \frac{\Im_{\varepsilon_2}[f(x+h\varepsilon_1+h\varepsilon_2)]}{h}, \quad (5)$$

and the second derivative $f''(x)$ can be obtained by taking the coefficient of $\varepsilon_1\varepsilon_2$ as

$$f''_{\mathrm{HDSD}}(x) = \frac{\Im_{\varepsilon_1\varepsilon_2}[f(x+h\varepsilon_1+h\varepsilon_2)]}{h^2}. \quad (6)$$

Because the expressions given in Eqs. (5) and (6) do not include subtraction or higher-order terms $O(h^3)$, the results do not contain roundoff or truncation errors.

The extension of the HDSD method to higher-order HDNs is straightforward. As an example, to compute third-order derivatives, third-order HDNs are required, meaning three nilpotent elements ε_1, ε_2 and ε_3 are defined with the properties:

$$\varepsilon_1^2 = 0, \quad \varepsilon_2^2 = 0, \quad \varepsilon_3^2 = 0,$$
$$\varepsilon_1\varepsilon_2 = \varepsilon_2\varepsilon_1, \quad \varepsilon_2\varepsilon_3 = \varepsilon_3\varepsilon_2, \quad \varepsilon_3\varepsilon_1 = \varepsilon_1\varepsilon_3,$$
$$\varepsilon_1\varepsilon_2\varepsilon_3 = \varepsilon_2\varepsilon_3\varepsilon_1 = \varepsilon_3\varepsilon_1\varepsilon_2 = \varepsilon_2\varepsilon_1\varepsilon_3 = \varepsilon_1\varepsilon_3\varepsilon_2 = \varepsilon_3\varepsilon_2\varepsilon_1 . \tag{7}$$

Analogously, fourth-order derivatives require four nilpotent elements ε_1, ε_2, ε_3 and ε_4. An extension of the above discussion reveals that any nth-order HDN requires 2^n coefficients and accordingly requires the corresponding computational efforts. In this report, the operations $\mathfrak{I}_{\varepsilon_3}$, $\mathfrak{I}_{\varepsilon_4}$ and $\mathfrak{I}_{\varepsilon_3\varepsilon_4}$ of taking the coefficients of the third- and fourth-order HDNs are defined as follows. A new number system is defined with $c = c_1 + c_2\varepsilon_3 + c_3\varepsilon_4 + c_4\varepsilon_3\varepsilon_4$, where c_i $(i = 1, 2, 3, 4)$ represents the coefficients in the second-order HDN c as $c_i = c_{i1} + c_{i2}\varepsilon_1 + c_{i3}\varepsilon_2 + c_{i4}\varepsilon_1\varepsilon_2$ and $c_{ij} \in \mathbb{R}$ $(j = 1, 2, 3, 4)$. Then, $\mathfrak{I}_{\varepsilon_3}[c] = c_2$, $\mathfrak{I}_{\varepsilon_4}[c] = c_3$ and $\mathfrak{I}_{\varepsilon_3\varepsilon_4}[c] = c_4$.

The above formulations can also be used for tensorvalued derivatives. Because of limited space, this report only discusses the application of the HDSD scheme. As examples of second-order tensors, $\boldsymbol{A}_1$ and $\boldsymbol{A}_2$ were defined as arbitrary second-order tensors on $\mathbb{R}^2$ or $\mathbb{R}^3$. Then, the directional derivative of a scalar function $z(\boldsymbol{X})$ of a second-order tensor argument $\boldsymbol{X}$ in the directions of $\boldsymbol{A}_1$ and $\boldsymbol{A}_2$ is given by

$$\partial_{\boldsymbol{X}} z : \boldsymbol{A}_1 = \mathfrak{I}_{\varepsilon_1}[z(\boldsymbol{X} + \varepsilon_1\boldsymbol{A}_1 + \varepsilon_2\boldsymbol{A}_2)],$$
$$\boldsymbol{A}_1 : \partial^2_{\boldsymbol{XX}} z : \boldsymbol{A}_2 = \mathfrak{I}_{\varepsilon_1\varepsilon_2}[z(\boldsymbol{X} + \varepsilon_1\boldsymbol{A}_1 + \varepsilon_2\boldsymbol{A}_2)], \tag{8}$$

where $\partial_{\boldsymbol{X}}$ and $\partial^2_{\boldsymbol{XX}}$ indicate first and second partial derivatives with respect to $\boldsymbol{X}$, respectively.

3. Application of Hyper-dual Step Derivative Scheme to Calculation of Stress and Tangent Modulus

The existence of a Helmholtz free energy function $\psi := \psi(\boldsymbol{C})$ or $\psi := \psi(\boldsymbol{E})$ with the right Cauchy-Green deformation tensor $\boldsymbol{C}$ and the Green-Lagrange strain tensor $\boldsymbol{E}$ was assumed. The constitutive equation could then be obtained via ψ as

$$\boldsymbol{S} = \frac{\partial \psi}{\partial \boldsymbol{E}} = 2\,\frac{\partial \psi}{\partial \boldsymbol{C}}, \tag{9}$$

and

$$\mathbb{C} = \frac{\partial \boldsymbol{S}}{\partial \boldsymbol{E}} = \frac{\partial^2 \psi}{\partial \boldsymbol{E}\,\partial \boldsymbol{E}} \text{ or } \mathbb{C} = 2\,\frac{\partial \boldsymbol{S}}{\partial \boldsymbol{C}} = 4\,\frac{\partial^2 \psi}{\partial \boldsymbol{C}\,\partial \boldsymbol{C}}, \tag{10}$$

where $\boldsymbol{S}$ is the second Piola-Kirchhoff stress tensor and $\mathbb{C}$ is the material tangent modulus. A new tensor $\overset{*}{\boldsymbol{C}}{}^{\mathrm{IJ}}$ was then defined as

$$\overset{*}{\boldsymbol{C}}{}^{\mathrm{IJ}} = \frac{1}{2}(\boldsymbol{E}^{\mathrm{I}} \otimes \boldsymbol{E}^{\mathrm{J}} + \boldsymbol{E}^{\mathrm{J}} \otimes \boldsymbol{E}^{\mathrm{I}}), \tag{11}$$

where $\boldsymbol{E}^I$ is Cartesian basis vector in the reference configuration and the italicized and non-italicized indices indicate tensor components and tensor directions, respectively. Then, by substituting ψ for z, $\boldsymbol{C}$ for $\boldsymbol{X}$, $\overset{*}{\boldsymbol{C}}{}^{\mathrm{IJ}}$ for $\boldsymbol{A}$, and $\overset{*}{\boldsymbol{C}}{}^{\mathrm{KL}}$ for $\boldsymbol{B}$ in Eq. (8), the numerical stress and tangent modulus could be obtained for the HDSD scheme as

$$S^{IJ}_{\mathrm{HDSD}} = 2\,\frac{\mathfrak{I}_{\varepsilon_1}[\psi(\boldsymbol{C} + h_S\,\varepsilon_1\overset{*}{\boldsymbol{C}}{}^{\mathrm{IJ}})]}{h_S}, \tag{12}$$

$$\mathbb{C}^{IJKL}_{\mathrm{HDSD}} = 4\,\frac{\mathfrak{I}_{\varepsilon_1\varepsilon_2}[\psi(\boldsymbol{C} + h_S\,\varepsilon_1\overset{*}{\boldsymbol{C}}{}^{\mathrm{IJ}} + h_C\,\varepsilon_2\overset{*}{\boldsymbol{C}}{}^{\mathrm{KL}})]}{h_S h_C}, \tag{13}$$

where h_S and h_C are the perturbation values in the calculation of the stress and tangent modulus, respectively.

4. Incremental Variational Formulation

The IVF provides a general framework for a broad range of constitutive equations.[11,20] In this formulation, the effective potential W^{eff} in a given time interval $[t_n, t_{n+1}]$ is defined as

$$W^{\mathrm{eff}} := \inf_{\boldsymbol{q}_{n+1}} W(\boldsymbol{F}_{n+1}, \boldsymbol{q}_{n+1}), \tag{14}$$

where $\boldsymbol{q}_{n+1}$ is the collocation of internal variables at the current time t_{n+1} and ϕ is the dissipation potential. Here, the incremental potential energy W is given by

$$W(\boldsymbol{F}_{n+1}, \boldsymbol{q}) := \int_{t_n}^{t_{n+1}} (\dot{\psi}(\boldsymbol{F}_{n+1}, \boldsymbol{q}) + \phi(\boldsymbol{q}, \dot{\boldsymbol{q}}))\,dt, \tag{15}$$

and its discretized counterpart is given by

$$W(\boldsymbol{F}_{n+1}, \boldsymbol{q}_{n+1}) = \psi(\boldsymbol{F}_{n+1}, \boldsymbol{q}_{n+1}) - \psi(\boldsymbol{F}_n, \boldsymbol{q}_n) + \Delta t\,\phi\left(\boldsymbol{q}_{n+1}, \frac{\Delta \boldsymbol{q}}{\Delta t}\right), \tag{16}$$

where the increment of the internal variable is defined as $\Delta\boldsymbol{q} = \boldsymbol{q}_{n+1} - \boldsymbol{q}_n$ and is assumed to be constant in the time increment $\Delta t := t_{n+1} - t_n$. The minimization problem given in Eq. (14) is solved using the Newton-Raphson iterative method, and $\boldsymbol{q}_{n+1}$ is obtained by iterating

$$\boldsymbol{q}^{(m+1)}_{n+1} = \boldsymbol{q}^{(m)}_{n+1} - (\partial^2_{\boldsymbol{qq}} W^{(m)})^{-1}\,\partial_{\boldsymbol{q}} W^{(m)}, \quad m = 0, 1, 2, \ldots, \tag{17}$$

until it converges, where (m) denotes the iteration number in the Newton-Raphson method.

With this updated internal variable $\boldsymbol{q}_{n+1}$, the stress $\boldsymbol{P}_{n+1}$ and corresponding consistent tangent modulus $\mathbb{A}_{n+1}$ at time t_{n+1} are computed as

$$\boldsymbol{P}_{n+1} = \partial_{\boldsymbol{F}_{n+1}} W^{\mathrm{eff}}(\boldsymbol{F}_{n+1}, \boldsymbol{q}_{n+1}(\boldsymbol{F}_{n+1})) , \tag{18}$$

$$\mathbb{A}_{n+1} = \partial^2_{\boldsymbol{F}_{n+1}\boldsymbol{F}_{n+1}} W^{\mathrm{eff}}(\boldsymbol{F}_{n+1}, \boldsymbol{q}_{n+1}(\boldsymbol{F}_{n+1})) . \tag{19}$$

Note that $\boldsymbol{q}_{n+1}$ is a function of the deformation gradient $\boldsymbol{F}_{n+1}$ and derivatives up to at least fourth-order with respect to $\boldsymbol{F}_{n+1}$ and $\boldsymbol{q}_{n+1}$ are required to compute the stresses and tangent moduli via Eqs. (17)-(19). Because the IVF is similar to the hyperelastic formulation, it is also called "the quasi-hyperelastic formulation." The algorithm is summarized in **Fig. 1**.

5. Numerical Examples

In this section, the performance of the proposed implementation scheme is demonstrated by applying it to some numerical examples. This section focuses on two material models, an anisotropic polyconvex hyperelastic model proposed by Balzani[21] and a finite strain elastoplastic model using the classical von Mises yield function including linear isotropic hardening, which is based on a multiplicative decomposition of the deformation gradient.[22,23] The proposed IVF scheme (Fig. 1) was implemented in the general-purpose finite-element software FEAP, developed by R. L. Taylor (www.ce.berkeley.edu/projects/feap/).

5. 1 Anisotropic Hyperelastic Materials

The anisotropic polyconvex hyperelastic model is given by

1. Database $\boldsymbol{q}_n$ and $\boldsymbol{F}_{n+1}$ are given.
2. Compute stress and tangent modulus.

   Loop over $i, j, k, l = \{1, 2, 3\}$:

   2. 1 Perturb deformation gradient $\overset{*}{\boldsymbol{F}}_{n+1} = \boldsymbol{F}_{n+1} + \varepsilon_1 \boldsymbol{A}_1^{\mathrm{ij}} + \varepsilon_2 \boldsymbol{A}_2^{\mathrm{kl}}$.

   2. 2 Set $m = 0$ and initialize $\overset{*}{\boldsymbol{q}}{}^{(m=0)}_{n+1} = \boldsymbol{q}_n$

   2. 3 Compute effective stress potential $\overset{**}{W}{}^{\mathrm{eff}} = \inf_{\boldsymbol{q}_{n+1}} W$ and internal variables $\overset{*}{\boldsymbol{q}}_{n+1}$:

      Loop over $m = 0, 1, \cdots$:

      2. 3. 1 Compute $\partial_{\boldsymbol{q}} \overset{**}{W}{}^{(m)}$ and $\partial^2_{\boldsymbol{qq}} \overset{*}{W}{}^{(m)}$:

         Loop over $r, s = \{1, 2, \cdots \dim[\boldsymbol{q}]\}$:

         2. 3. 1. 1 Perturb internal variables: $\overset{**}{\boldsymbol{q}}{}^{(m)}_{n+1} = \overset{*}{\boldsymbol{q}}{}^{(m)}_{n+1} + \varepsilon_3 \boldsymbol{\alpha}^r + \varepsilon_4 \boldsymbol{\alpha}^s$.

         2. 3. 1. 2 Evaluate function: $\overset{**}{W}{}^{(m)} = W(\overset{*}{\boldsymbol{F}}_{n+1}, \overset{**}{\boldsymbol{q}}{}^{(m)}_{n+1})$.

         2. 3. 1. 3 Compute first derivative $(\partial_{\boldsymbol{q}} \overset{*}{W}{}^{(m)})_r = \Im_{\varepsilon_3}[\overset{**}{W}{}^{(m)}]$.

         2. 3. 1. 4 Compute second derivative $(\partial^2_{\boldsymbol{qq}} \overset{*}{W}{}^{(m)})_{rs} = \Im_{\varepsilon_3\varepsilon_4}[\overset{**}{W}{}^{(m)}]$.

      2. 3. 2 Convergence check: If $(\left\| \Re[\partial_{\boldsymbol{q}} \overset{*}{W}{}^{(m)}] \right\| < tol)$ go to 2.4.

      2. 3. 3 Perform Newton update: $\overset{*}{\boldsymbol{q}}{}^{(m+1)}_{n+1} = \overset{*}{\boldsymbol{q}}{}^{(m)}_{n+1} - (\partial^2_{\boldsymbol{qq}} \overset{*}{W}{}^{(m)})^{-1} \partial_{\boldsymbol{q}} \overset{*}{W}{}^{(m)}$

   2. 4 Calculate stress and tangent modulus:

   $(\boldsymbol{P}_{n+1})_{ij} = \Im_{\varepsilon_1}[\overset{**}{W}{}^{\mathrm{eff}}]$ and $(\mathbb{A}_{n+1})_{ijkl} = \Im_{\varepsilon_1\varepsilon_2}[\overset{**}{W}{}^{\mathrm{eff}}]$.

3. Update database $\boldsymbol{q}_{n+1} = \Re[\overset{*}{\boldsymbol{q}}_{n+1}]$.

Fig. 1 Algorithm for computation of IVF using HDNs.

$$\psi = \alpha_1(I_1 I_3^{-1/3} - 3) + \alpha_2(I_3^{\alpha_3} + I_3^{-\alpha_3} - 2) + \sum_{a=1}^{n_f} \left[\beta_1 \langle I_1 J_4^{(a)} - J_5^{(a)} - 2 \rangle^{\beta_2}\right], \quad (20)$$

where the isotropic part describes the ground substance and the anisotropic part represents the embedded fibers.[21] The material parameters $\alpha_1 > 0$, $\alpha_2 > 0$, $\alpha_3 > 0$, $\beta_1 > 0$ and $\beta_2 > 2$ are determined from the least-squares fitting of the experimental data, and n_f shows the number of fiber families. In Eq. (20), $\langle \bullet \rangle$ denotes the Macaulay bracket and $I_1 = \mathrm{tr}[\boldsymbol{C}]$, $I_3 = \det[\boldsymbol{C}]$, $J_4^{(a)} = \mathrm{tr}[\boldsymbol{C}\boldsymbol{M}_{(a)}]$ and $J_5^{(a)} = \mathrm{tr}[\boldsymbol{C}^2\boldsymbol{M}_{(a)}]$ are the principal invariants with the structural tensor $\boldsymbol{M}_{(a)} = \boldsymbol{a}_{0(a)} \otimes \boldsymbol{a}_{0(a)}$, where $\boldsymbol{a}_{0(a)}$ represents the fiber direction.

For the first investigation, a homogeneous test was conducted with a specific deformation gradient $\boldsymbol{F}$, which includes rotations $\boldsymbol{Q}$, dilation, and shear deformation $\boldsymbol{F}_0$ as

$$\boldsymbol{F} = \boldsymbol{Q}\boldsymbol{F}_0 \text{ with } \boldsymbol{Q} = \boldsymbol{R}_{\theta_1}\boldsymbol{R}_{\theta_2}\boldsymbol{R}_{\theta_3}. \quad (21)$$

In this example, these deformations are defined as

$$\boldsymbol{R}_{\theta_1} = \begin{bmatrix} \cos\frac{\pi}{4} & -\sin\frac{\pi}{4} & 0 \\ \sin\frac{\pi}{4} & \cos\frac{\pi}{4} & 0 \\ 0 & 0 & 1 \end{bmatrix},$$

$$\boldsymbol{R}_{\theta_2} = \begin{bmatrix} \cos\frac{\pi}{3} & 0 & \sin\frac{\pi}{3} \\ 0 & 1 & 0 \\ -\sin\frac{\pi}{3} & & \cos\frac{\pi}{3} \end{bmatrix},$$

$$\boldsymbol{R}_{\theta_3} = \begin{bmatrix} 1 & 0 & 0 \\ 0 & \cos\frac{\pi}{6} & -\sin\frac{\pi}{6} \\ 0 & \sin\frac{\pi}{6} & \cos\frac{\pi}{6} \end{bmatrix},$$

$$\boldsymbol{F}_0 = \begin{bmatrix} 1.1 & \gamma & \gamma \\ 0 & 0.9535 & \gamma \\ 0 & 0 & 0.9535 \end{bmatrix}, \quad (22)$$

where γ implies the amplitude of the shear deformation. The material parameters were defined as follows: $\alpha_1 = 1.0$, $\alpha_2 = 1.0$, $\alpha_3 = 0.1$, $\beta_1 = 1.0$ and $\beta_2 = 3.0$. Additionally, the number of preferred directions was defined as $n_f = 2$ with $\boldsymbol{a}_{0(1)} = 1/3(1\ 2\ 2)^T$ and $\boldsymbol{a}_{0(2)} = 1/\sqrt{5}(2\ 1\ 0)^T$. For the hyperelastic material models, the minimization problem given in Eq. (14) was not considered, because the effective potential is equal to the strain energy function given by Eq. (20). The numerical results for the tangent modulus computed using the FD method, the CSDA method starting with the stress tensor, and the HDSD method Eq. (13) starting from the strain energy function Eq. (20) were compared with an analytically derived tangent modulus.[6] The relative error $e_{\mathbb{C}}$ was defined as

$$e_{\mathbb{C}} = \sqrt{\frac{\sum_{I,J,K,L} ((\mathbb{C}_{\mathrm{analyt}})^{IJKL} - (\mathbb{C}_{\mathrm{approx}})^{IJKL})^2}{\sum_{I,J,K,L} ((\mathbb{C}_{\mathrm{analyt}})^{IJKL})^2}}, \quad (23)$$

where $(\mathbb{C}_{\mathrm{analyt}})^{IJKL}$ are the coefficients of the analytic material tangent modulus and $(\mathbb{C}_{\mathrm{approx}})^{IJKL}$ are their approximations. **Figure 2** shows the accuracy of each numerical approximation scheme. The FD method is quite sensitive to the perturbation value and can obtain an optimal accuracy of $e_{\mathbb{C}} \approx 10^{-7}$ with $h \approx 10^{-7}$. Increasing or decreasing the perturbation value from this value increases the error. The CSDA approach is able to achieve an error with computer accuracy at perturbation values smaller than approximately 10^{-9}. The HDSD error is independent of the perturbation value and always achieves computer accuracy.

As a second investigation, a Cook-type cantilever beam was considered, as schematically illustrated in **Fig. 3**(a). Here, only one fiber family ($n_f = 1$) with $\boldsymbol{a}_{(1)} = 1/\sqrt{3}\ (1\ 1\ 1)^T$ was embedded. The material parameters were set as follows: $\alpha_1 = 6.0$, $\alpha_2 = 100.0$, $\alpha_3 = 5.0$, $\beta_1 = 100.0$ and $\beta_2 = 2.5$. The maximum load p_0 was increased until the ultimate maximum load of $p_0 = 5.0$ was reached. First, the HDSD scheme with Eqs. (12) and (13) was applied to directly compute both the stress and tangent modulus from the strain energy function Eq. (20). Second, the FD scheme was applied twice as an alternative method of numerically computing the stress and modulus from Eq. (20). Third, the analytically derived expression for the

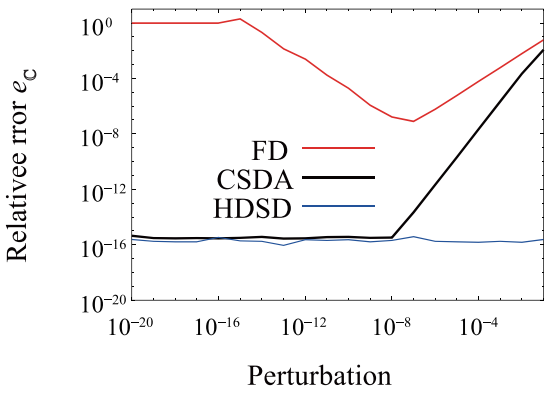

Fig. 2 Relative errors $e_{\mathbb{C}}$ of tangent moduli approximated using the FD, CSDA, and HDSD methods.

stress was used in combination with the tangent modulus numerically computed using the CSDA scheme. The resulting Kirchhoff stress distributions τ_{11} at the ultimate maximum load $p_0 = 5.0$ are shown in Fig. 3(b). The stress distributions obtained using all of these numerical differentiation schemes were found to be very similar to the analytically derived stress and modulus.

The Euclidean norms of the residuals obtained using the FD method with different perturbation values h_S and h_C and the HDSD schemes with $h_S = 1.0$ and $h_C = 1.0$ are given in **Table 1**. Whereas the HDSD results yield residuals that are almost equivalent to those obtained using an analytic implementation of the stress and tangent modulus, the FD results differ by orders of magnitude at all considered perturbation values, and the quadratic convergence can hardly be distinguished.

The computational costs of the different numerical differentiation schemes are compared in **Fig. 4**. As expected, the computation time of the FD method is dependent on the perturbation value and is optimized at perturbation values of $h_S = 10^{-4}$ and $h_C = 10^{-6}$. The HDSD method is only slightly slower than the bestperforming FD method and is faster than the FD method with certain numbers of elements. It is worth

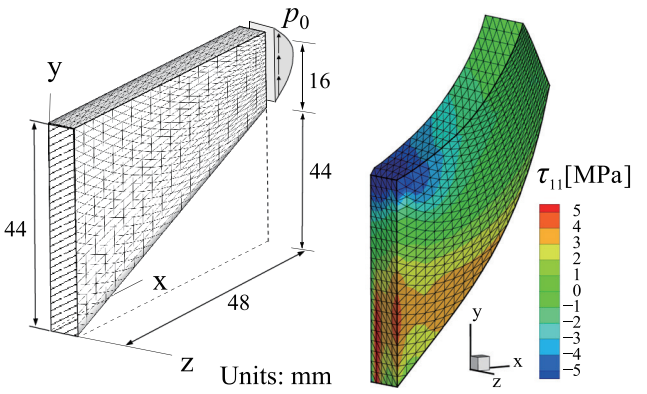

(a) Boundary value problem (b) Stress distribution

Fig. 3 Description of Cook-type cantilever beam and resulting deformed configuration with stress distribution.

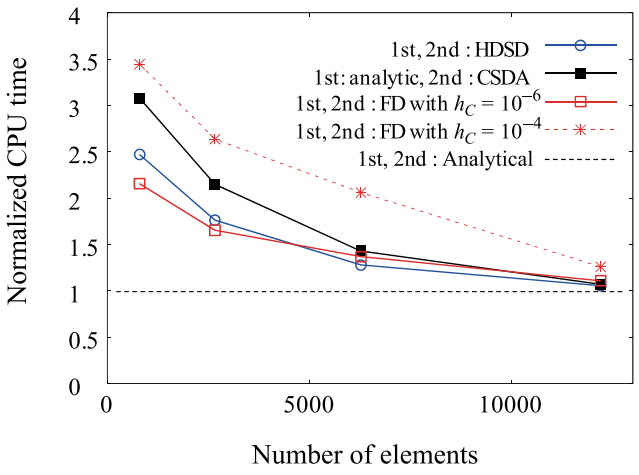

Fig. 4 Comparison of computational times of different numerical differentiation methods for Cook-type problem.

Table 1 Euclidean norms of residuals of Cook-type problem obtained using the FD and HDSD schemes.

Analytical	FD with $h_S = 10^{-4}$			HDSD
	$h_C = 10^{-4}$	$h_C = 10^{-6}$	$h_C = 10^{-8}$	
5.4504×10^{-1}	6.3167×10^{1}	6.3167×10^{1}	6.3167×10^{1}	5.4504×10^{-1}
$1.8568 \times 10^{+2}$	9.3803×10^{1}	9.0099×10^{1}	9.0116×10^{1}	1.8568×10^{2}
$1.5341 \times 10^{+0}$	2.0612×10^{0}	2.4092×10^{0}	2.4096×10^{0}	1.5341×10^{0}
$3.4458 \times 10^{+0}$	3.2625×10^{0}	3.2628×10^{0}	3.2630×10^{0}	3.4458×10^{0}
8.4932×10^{-3}	6.5687×10^{-3}	1.4598×10^{-2}	1.4692×10^{-2}	8.4932×10^{-3}
2.0186×10^{-4}	4.2600×10^{-4}	5.3153×10^{-4}	5.7587×10^{-4}	2.0187×10^{-4}
5.0665×10^{-8}	2.3998×10^{-5}	2.0946×10^{-6}	5.5211×10^{-6}	5.0161×10^{-8}
–	2.3392×10^{-6}	3.3563×10^{-7}	3.3765×10^{-7}	–
–	4.2348×10^{-7}	–	–	–
–	3.3564×10^{-7}	–	–	–

emphasizing that the optimal perturbation values are generally unknown, meaning the FD method can typically be expected to be much slower than the HDSD method because the optimal perturbation values are likely not used. Moreover, the HDSD method is also faster than the CSDA method, although both the first and second derivatives are calculated numerically in the HDSD method, whereas the CSDA scheme requires an analytic expressions for the stress.

5. 2 Associative Elastoplastic Material Models at Finite Strain

In this numerical example, a finite-strain elastoplastic material model was applied using the von Mises yield function including exponential isotropic hardening.[24,25] The multiplicative decomposition $\boldsymbol{F} = \boldsymbol{F}^{\mathrm{e}} \cdot \boldsymbol{F}^{\mathrm{p}}$ with $\det \boldsymbol{F}^{\mathrm{p}} = 1$ of the deformation gradient $\boldsymbol{F}$ into elastic and plastic parts $\boldsymbol{F}^{\mathrm{e}}$ and $\boldsymbol{F}^{\mathrm{p}}$ with $\det \boldsymbol{F}^{\mathrm{p}} = 1$ and the additive decomposition $\psi = \psi^{\mathrm{e}} + \psi^{\mathrm{p}}$ of the Helmholtz energy ψ into elastic and plastic parts ψ^{e} and ψ^{p} were applied in this study. The elastic response is defined as

$$\psi^{\mathrm{e}} = \frac{\lambda}{2}[b_1^{\mathrm{e}} + b_2^{\mathrm{e}} + b_3^{\mathrm{e}}]^2 + \mu[(b_1^{\mathrm{e}})^2 + (b_2^{\mathrm{e}})^2 + (b_3^{\mathrm{e}})^2], \quad (24)$$

where λ and μ are material parameters and b_A^{e} (A = 1, 2, 3) is the logarithm of the eigenvalue λ_A^{e} of the elastic left Cauchy-Green deformation tensor $\boldsymbol{b}^{\mathrm{e}} = \boldsymbol{F}^{\mathrm{e}}\boldsymbol{F}^{\mathrm{e}T}$ as $b_A^{\mathrm{e}} = \log(\lambda_A^{\mathrm{e}})$. The plastic response is defined as

$$\psi^{\mathrm{p}} = y_\infty \alpha - \frac{1}{\eta}(y_0 - y_\infty)e^{-\eta\alpha} + \frac{1}{2}H\alpha^2, \quad (25)$$

where α is an isotropic hardening variable, y_∞ is the initial yield strength, y_0 is the plastic yield strength at the initialization of linear hardening, η is the degree of exponential hardening, and H is the slope of superimposed linear hardening. The collocation set $\boldsymbol{q}$ of the internal variables is defined as

$$\boldsymbol{q} = [\boldsymbol{F}^{\mathrm{p}},\ \alpha]^T. \quad (26)$$

The conjugate internal force vector $\boldsymbol{y}$ of $\boldsymbol{q}$ is

$$\boldsymbol{y} := -\frac{\partial \psi}{\partial \boldsymbol{q}} = \left[-\frac{\partial \psi^{\mathrm{e}}}{\partial \boldsymbol{F}^{\mathrm{p}}}, -\frac{\partial \psi^{\mathrm{p}}}{\partial \alpha}\right]^T = \left[\boldsymbol{\Sigma}\boldsymbol{F}^{\mathrm{p}-T}, \beta\right]^T, \quad (27)$$

where $\boldsymbol{\Sigma}$ is the Mandel stress tensor and β is the thermodynamic conjugate force of α. The dissipation potential ϕ is defined using the maximum dissipation principle (MDP) as

$$\phi = \sup_{(\Sigma_{n+1},\, \beta_{n+1}) \in \mathbb{E}} [\boldsymbol{\Sigma}_{n+1} : \Delta\boldsymbol{L}^{\mathrm{p}} + \beta_{n+1} \cdot \Delta\alpha], \quad (28)$$

where $\Delta\boldsymbol{L}^{\mathrm{p}}$ is the constant plastic velocity gradient in the current time increment and $\Delta\alpha := \alpha_{n+1} - \alpha_n$. The elastic domain $\mathbb{E}$ is restricted using the yield function Y as

$$\mathbb{E} := \{(\boldsymbol{\Sigma}, \beta) \mid Y(\boldsymbol{\Sigma}, \beta) = \| \operatorname{dev} \boldsymbol{\Sigma} \| - \sqrt{2/3}\beta \le 0\}, \quad (29)$$

where dev(•) is the deviatoric operator. Through the use of Karush-Kuhn-Tucker (KKT) conditions, the inf-sup problem given by Eq. (14) and Eq. (28) can be rewritten as one parameter minimization problem using the Lagrange multiplier $\Delta\gamma$[26] as

$$W^{\mathrm{eff}} = \inf_{\Delta\gamma \ge 0} [\psi(\boldsymbol{F}_{n+1}, \Delta\gamma) - \psi(\boldsymbol{F}_n) + \Delta\gamma Y] \quad \text{with} \quad \Delta\gamma Y = 0, \quad Y \le 0, \quad (30)$$

with the updating

$$\boldsymbol{F}_{n+1}^{\mathrm{p}} = \exp\left(\Delta\gamma \frac{\partial Y}{\partial \boldsymbol{\Sigma}}\right) \cdot \boldsymbol{F}_n^{\mathrm{p}},$$
$$\alpha_{n+1} = \alpha_n + \Delta\gamma \frac{\partial Y}{\partial \boldsymbol{\Sigma}}. \quad (31)$$

To demonstrate the performance of the proposed HDSD-based IVF scheme for the finite-strain elastoplastic model, its application to a statistically similar representative volume element (SSRVE) of a dual-phase (DP) steel microstructure was investigated. The SSRVE depicted in **Fig. 5**(a), which is as statistically similar as possible to the real random microstructure,[2] was considered in this investigation. In this model, the material parameters in **Table 2** were used to represent a ferritic matrix phase with an embedded martensitic inclusion phase in a typical DP steel microstructure. The application of a macroscopic shear deformation $\bar{\boldsymbol{F}}$ to the SSRVE and periodic boundary conditions were considered.

The resulting macroscopic stress-strain response and deformed configurations of the SSRVE with stress distributions τ_{23} are depicted in **Fig. 6**, Figs. 5(b) and (c), respectively. Both the macro- and microscopic results depicted in these figures show good agreement between the proposed HDSD-based implementation

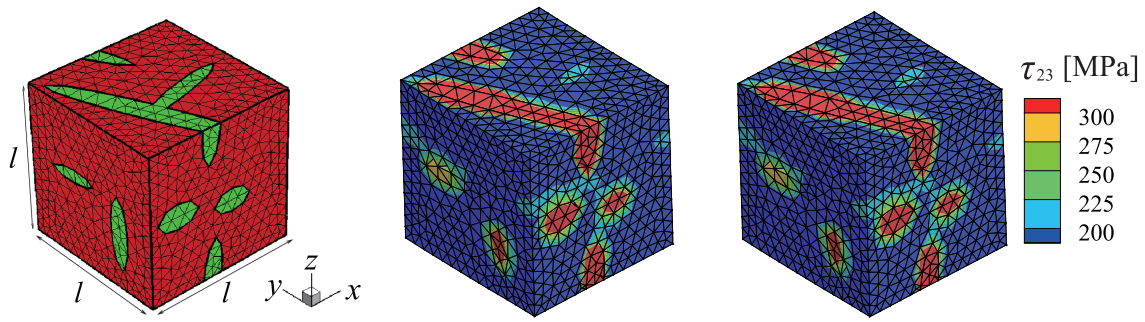

(a) Geometry, l = 5 μm (b) Standard return mapping (c) IVF with HDSD

Fig. 5 Description of SSRVE and deformed configurations obtained using the classical standard return mapping method and the proposed HDSD-based IVF scheme.

Table 2 Material parameters for individual phases of DP steel microstructure.

	λ [MPa]	μ [MPa]	y_0 [MPa]	y_∞ [MPa]	η [--]	H [MPa]
Matrix (Ferrite)	118,846.2	79,230.77	260.0	580.0	9.0	70.0
Inclusion (Martensite)	118,846.2	79,230.77	1000.0	2750.0	35.0	10.0

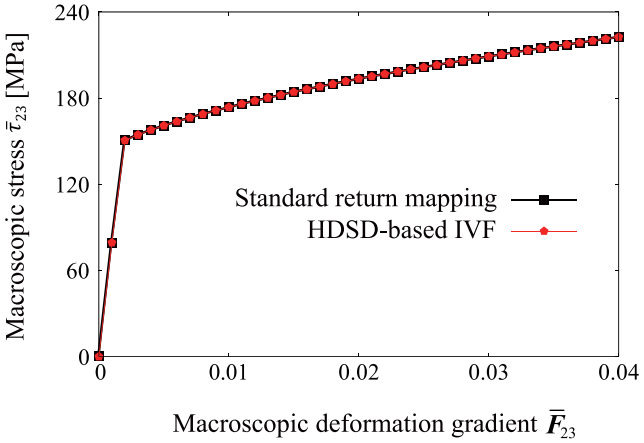

Fig. 6 Macroscopic stress-strain diagram for simple shear deformation of SSRVE of DP steel microstructure.

scheme and the classical standard return mapping scheme. It is worth noting that the proposed implementation scheme has a general structure that has been defined such that once the present framework is constructed, only scalarvalued quantities, such as the free energy function ψ and the dissipative function ϕ and the yield function Y, require modification, even for the consideration of any other complicated constitutive equations.

6. Conclusion

This report proposed a novel scheme for the implantation of a broad range of constitutive equations in general-purpose finite element software. The proposed scheme involves the automatic calculation of stresses and their corresponding tangent moduli using an IVF and the HDSD. In the IVF, the unknown internal variables are determined by solving a minimization problem that consists of an incrementally defined potential. The present stresses and corresponding tangent moduli can be obtained by differentiating the minimized effective potential with respect to the present deformation gradient. In this study, the HDSD scheme was applied to automatically compute the differentiations needed in the IVF.

The proposed implementation scheme has a general structure that is defined such that once the present framework has been constructed, any other complicated constitutive equations can be considered by simply modifying scalar-valued quantities, such as the Helmholtz free energy function, the dissipation potential, and the additional yield function in the case of plasticity.

The proposed implementation scheme was demonstrated to be extremely robust, accurate, and

userfriendly for any elastic or inelastic material model. The proposed scheme will be particularly useful in the scientific development of multiscale material models, which can be used to help ensure the safety and reliability of vehicles from a materials science perspective.

Acknowledgments

The authors are particularly grateful to Prof. Jörg Schröder (University of Duisburg-Essen, Germany), Prof. Daniel Balzani (TU Dresden, Germany), and Dr. Masaki Fujikawa (University of the Ryukyus, Japan) for their support and fruitful discussion, which helped in the successful completion of this research project.

References

(1) Schröder, J., "A Numerical Two-scale Homogenization Scheme: the FE^2-method", *Plasticity and Beyond – Microstructures, Crystal-plasticity and Phase Transitions* (2013), pp. 1-64, Springer.
(2) Balzani, D., Scheunemann, L., Brands, D. and Schröder, J., "Construction of Two- and Three-dimensional Statistically Similar RVEs for Coupled Micro-macro Simulations", *Comput. Mech.*, Vol. 54 (2014), pp. 1269-1284.
(3) Pérez-Foguet, A., Rodríguez-Ferran, A. and Huerta, A., "Numerical Differentiation for Local and Global Tangent Operators in Computational Plasticity", *Comput. Methods Appl. Mech. Eng*., Vol. 189 (2000), pp. 277-296.
(4) Pérez-Foguet, A., Rodríguez-Ferran, A. and Huerta, A., "Numerical Differentiation for Non-trivial Consistent Tangent Matrices: An Application to the MRS-lade Model", *Int. J. Numer. Methods Eng*., Vol. 48 (2000), pp. 159-184.
(5) Kim, S., Ryu, J. and Cho, M., "Numerically Generated Tangent Stiffness Matrices Using the Complex Variable Derivative Method for Nonlinear Structural Analysis", *Comput. Methods Appl. Mech. Eng*., Vol. 200 (2011), pp. 403-413.
(6) Tanaka, M., Fujikawa, M., Balzani, D. and Schröder, J., "Robust Numerical Calculation of Tangent Moduli at Finite Strains Based on Complex-step Derivative Approximation and Its Application to Localization Analysis", *Comput. Methods Appl. Mech. Eng*., Vol. 269 (2014), pp. 454-470.
(7) Kiran, R. and Khandelwal, K., "Complex Step Derivative Approximation for Numerical Evaluation of Tangent Moduli", *Comput. Struct*., Vol. 140 (2014), pp. 1-13.
(8) Balzani, D., Gandhi, A., Tanaka, M. and Schröder, J., "Numerical Calculation of Thermo-mechanical Problems at Large Strains Based on Robust Approximations of Tangent Stiffness Matrices", *Comput. Mech*., Vol. 55 (2015), pp. 861-871.
(9) Hürkamp, A., Tanaka, M. and Kaliske, M., "Complex Step Derivative Approximation of Consistent Tangent Operators for Viscoelasticity Based on Fractional Calculus", *Comput. Mech*., Vol. 56 (2015), pp. 1055-1071.
(10) Miehe, C., "Numerical Computation of Algorithmic (Consistent) Tangent Moduli in Large-strain Computational Inelasticity", *Comput. Methods Appl. Mech. Eng*., Vol. 134 (1996), pp. 223-240.
(11) Ortiz, M. and Stainier, L., "The Variational Formulation of Viscoplastic Constitutive Updates", *Comput. Methods Appl. Mech. Eng*., Vol. 171 (1999), pp. 419-444.
(12) Yang, Q., Stainier, L. and Ortiz, M., "A Variational Formulation of the Coupled Thermo-mechanical Boundary-value Problem for General Dissipative Solids", *J. Mech. Phys. Solids*, Vol. 54 (2006), pp. 401-424.
(13) Stainier, L. and Ortiz, M., "Study and Validation of a Variational Theory of Thermo-mechanical Coupling in Finite Visco-plasticity", *Int. J. Solids Struct*., Vol. 47 (2010), pp. 705-715.
(14) Fike, J. A., "*Multi-objective Optimization Using Hyper-dual Numbers*", Ph.D. Thesis, Stanford University (2013).
(15) Tanaka, M., Sasagawa, T., Omote, R., Fujikawa, M., Balzani, D. and Schröder, J., "A Highly Accurate 1st- and 2nd-order Differentiation Scheme for Hyperelastic Material Models Based on Hyper-dual Numbers", *Comput. Methods Appl. Mech. Eng*., Vol. 283 (2015), pp. 22-45.
(16) Tanaka, M., Balzani, D. and Schröder, J., "Implementation of Incremental Variational Formulations Based on the Numerical Calculation of Ferivatives Using Hyper Dual Mumbers", *Comput. Methods Appl. Mech. Eng*., Vol. 301 (2016), p. 216-241.
(17) Lyness, J. N. "Differentiation Formulas for Analytic Functions", *Math.Comput*., pp. 352-362.
(18) Lai, K.-L. and Crassidis, J. L., "Extensions of the First and Second Complex-step Derivative Approximations", *J. Comput. Appl. Math*., Vol. 219 (2008), pp. 276-293.
(19) Martins, J. R. R. A. and Hwang, J. T., "Review and Unification of Discrete Methods for Computing Derivatives of Single- and Multi-disciplinary Computational Models", *AIAA J*., Vol. 51, No. 11 (2013), pp. 2582-2599.
(20) Miehe, C., "Strain-driven Homogenization of Inelastic Microstructures and Composites Based on an Incremental Variational Formulation", *Int. J. Numer. Methods Eng*., Vol. 55 (2002), pp. 1285-1322.
(21) Balzani, D., Neff, P., Schröder, J. and Holzapfel, G., "A Polyconvex Framework for Soft Biological Tissues – Adjustment to Experimental Data", *Int. J. Solids Struct*., Vol. 43, No. 20 (2006), pp. 6052- 6070.
(22) Kröner, E., "Allgemeine Kontinuumstheorie der

Versetzung und Eigenspannung", *Arch. Ration. Mech. Anal*., Vol. 4 (1960), pp. 273-334.
(23) Miehe, C., "Kanonische Modelle Multiplikativer Elasto-plastizität – Thermodynamische formulierung und Numerische Implementation", *Habilitation Thesis, Universität Hannover, Inst. Baumech. Numer. Mech*., No. F93/1.
(24) Mosler, J. and Bruhns, O., "Towards Variational Constitutive Updates for Non-associative Plasticity Models at Finite Strain: Models Based on a Volumetric-deviatoric Split", *Int. J. Solids Struct*., Vol. 46 (2009), pp. 1676-1684.
(25) Bleier, N. and Mosler, J., "Efficient Variational Constitutive Updates by Means of a Novel Parameterization of the Flow Rule", *Int. J. Numer. Methods Eng*., Vol. 89 (2012), pp. 1120-1143.
(26) Mosler, J. and Bruhns, O., "On the Implementation of Rate-independent Standard Dissipative Solids at Finite Strain – Variational Constitutive Updates", *Comput. Methods Appl. Mech. Eng*., Vol. 199 (2010), pp. 417-429.

Masato Tanaka
Research Fields:
- Nonlinear Material Modeling
- Finite Element Method

Academic Degree: Dr.Eng.
Academic Societies:
- The Japan Society of Mechanical Engineers
- The Japan Society for Computational Engineering and Science

Award:
- JSME Young Engineers Award, 2012

Takashi Sasagawa
Research Field:
- Material Modeling for Finite Element Analysis

Ryuji Omote
Research Fields:
- Numerical Modeling
- Material Strength
- Structural Mechanics

Academic Degree: Dr.Eng.
Academic Societies:
- The Japan Society of Mechanical Engineers
- The American Society of Mechanical Engineers